THE ASTROPHYSICAL JOURNAL, 394:188–195, 1992 July 20

ANOMALOUSLY HIGH APPARENT ABUNDANCES OF SINGLY IONIZED HELIUM IN THE GALACTIC H II REGION W3A

P. R. ROELFSEMA,[1] W. M. GOSS,[2] AND D. C. V. MALLIK[3]

Received 1991 August 30; accepted 1992 January 22

ABSTRACT

The distribution of singly ionized helium (Y^+) in the Galactic H II region W3A has been determined using high-resolution observations of radio recombination lines in the 76, 92, and 110α lines. The angular resolutions range from 2″ to 8″. In these lines, at frequencies between 14.7 to 4.9 GHz, the average Y^+ is found to vary from ~8% to ~12%. However, there are individual regions in W3A with Y^+ in excess of 20%. Enhancement of Y^+ due to underionization of hydrogen caused by the hardening of the radiation field is discussed. It is found that the high values of Y^+ cannot be due to variations in the ionization structure and thus must be due to a local enhancement of the helium abundance. A possible source of such enhancements might be an obscured evolved stellar object.

Subject headings: H II regions — ISM: abundances — ISM: individual (W3) — radio lines: atomic

1. INTRODUCTION

In recent years there have been a number of determinations of helium abundances in H II regions based on radio recombination line observations. Mezger (1980) has reviewed the extensive single-dish determinations and discussed the assumptions involved in determining the total helium abundance (Y) based on observations of radio recombination lines of singly ionized helium (Y^+). It is generally assumed that doubly ionized helium (Y^{++}) does not exist in H II regions; the exciting stars provide negligible ionization at energies above 54.4 eV. An important aspect in the interpretation of Y^+ as deduced from radio recombination line observations is the ionization structure of the H II region. In the presence of a relatively cool star (O8 and later), the He II region is smaller than the H II region. In such a case, the value of Y^+ will be less than Y because the He line is due to emission arising from a smaller volume than the H line. This effect is usually called the "geometric effect."

Helium abundance determinations from radio recombination lines have been used extensively to study possible helium abundance gradients throughout the Galaxy. Thum, Mezger, & Pankonin (1980) have suggested a slight gradient between 7 and 15 kpc. However, based on both radio and optical data, Shaver et al. (1983) found no significant gradient.

Interferometric observations of helium recombination lines with both the Westerbork Synthesis Radio Telescope (WSRT) and the Very Large Array (VLA) were carried out by Roelfsema (1987). In Sgr B2, Roelfsema et al. (1987) have found a significant decrease in Y^+ near the compact components in G0.7S; in all other components a value of Y^+ of about 10% was observed. This decrease in Y^+ could be explained by the geometric effect. For the various components in DR 21, Roelfsema, Goss, & Geballe (1990) observed variations in Y^+ from about 10% to <4%. Again, the geometric effect was involved due to the presence of a wide range of O stars (e.g., O6 and later).

In the direction of the H II region complex W3 ($l = 133.^\circ2$ $b = 1.^\circ2$ at a distance of 2.4 kpc), Roelfsema & Goss (1991) found a wide range of values of Y^+. In a number of small areas (<12″) in the west and southwest of component W3A (total size 40″; see Fig. 1) enhanced values of Y^+ in excess of 20% were observed at both 14.7 GHz (76α) and 4.9 GHz (110α). The components W3B, C, and D to the west of W3A show Y^+ values of 7.5% to 15%. Roelfsema & Goss (1991) do find slightly enhanced values of Y^+ of 15%–20% in the south of W3B. Bania, Rood, & Wilson (1987) report a high abundance of $^3He^+$ toward W3A ($^3He^+/H = 15 \times 10^{-5}$ as compared to a few 10^{-5} for most H II regions). Such a high $^3He^+$ abundance is consistent with a relatively high true helium abundance in the region.

In this paper, new high-sensitivity observations, using the new 8 GHz system at the VLA, are described. With a resolution of 8″, the locally enhanced helium lines have been confirmed at a third frequency.

2. OBSERVATIONS

The 76α and 110α data are taken from Roelfsema & Goss (1991). The 76α data at 14.7 GHz have an angular resolution of 1.″9 × 1.″4 (α × δ) and were obtained with the Very Large Array (VLA) in 1983–1984. The rms noise is 4.2 mJy beam^{-1}. The 110α data at 4.9 GHz have an angular resolution of 3.6 × 4.″2 (α × δ) and were obtained with the Westerbork Synthesis Radio Telescope (WSRT) in 1983; the rms noise is 1.8 mJy beam^{-1}.

In 1988 September, 92α observations (at 8.309383 GHz) were carried out over a 4 hr period. The D array of the VLA was used resulting in an angular resolution of 8″. A total bandwidth of 6.25 MHz (corresponding to 255 km s^{-1}), centered halfway between the H and He lines, with 63 channels was used. Thus a velocity resolution of 3.52 km s^{-1} is obtained. This configuration covers the H, He, and C recombination lines. (The velocity separation between H and He of 122.1 km s^{-1} corresponds to 3.4 MHz for 92α.) The rms noise is 2 mJy beam^{-1}.

3. RESULTS

In Figure 1 the W3 continuum image at 14.7 GHz (Roelfsema & Goss 1991) is shown with a resolution of 1.″9 × 1.″4 (α × δ). Within W3A, three areas (1, 2, and 3) are indi-

[1] Space Research Groningen, Postbus 800, 9700 AV, Groningen, The Netherlands.
[2] NRAO/VLA, P.O. Box 0, Socorro, NM, 87801.
[3] Indian Institute of Astrophysics, Bangalore, 5600321, India.

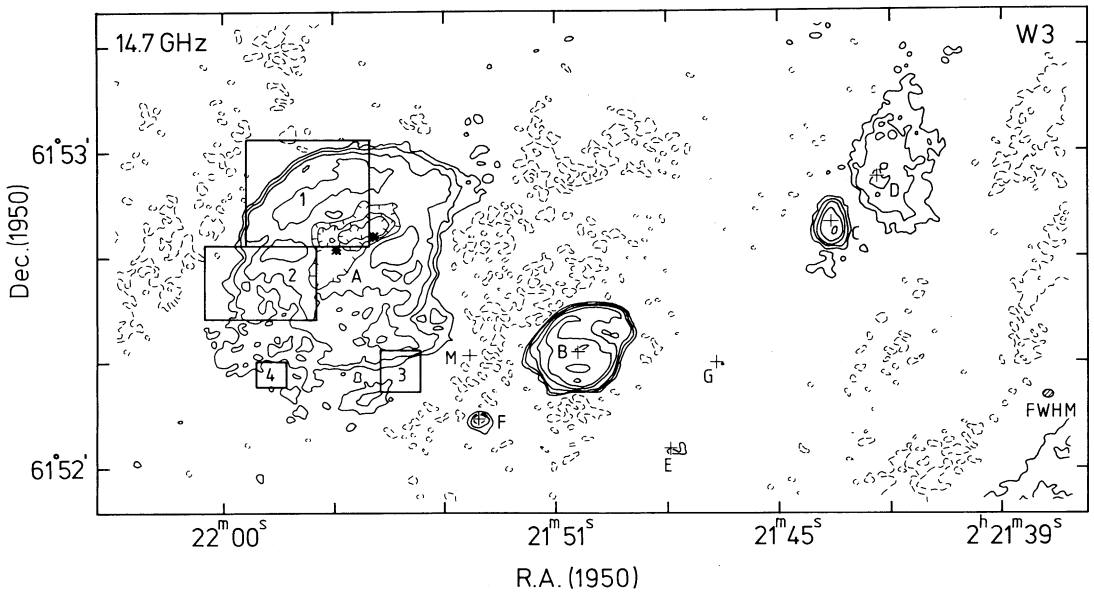

FIG. 1.—14.7 GHz continuum map of the W3 core region (from Roelfsema & Goss 1991). Contours are drawn at −5.6 (*dashed*), 5.6, 11, 22, 44, 89, and 177 mJy beam^{-1}. The noise level is 3.0 mJy beam^{-1}. 1 mJy beam^{-1} corresponds to 2.2 K. The resolution of 1.″9 × 1.″4 ($\alpha \times \delta$) is indicated by the hatched ellipse in the lower right-hand corner. The numbered boxes indicate the areas over which the data were integrated to obtain the spectra shown in Fig. 2.

cated with angular sizes of 8″–20″. Profiles obtained by averaging the line emission over each of these three areas are shown for the 76, 92, and 110α data in Figure 2. Gaussian profile fits to the data are shown as dashed lines; the results of these fits (line amplitude, velocity V_{lsr}, and FWHM ΔV_G) are summarized in Table 1 with estimated 1 σ errors within parentheses. For all profiles the H and He lines were fitted with a Gaussian. Additionally a C line was fitted for all 110α profiles as well as for the 92α profile toward region 3 (Fig. 2*c*). The C line appears to be somewhat broad ($\Delta V_G \sim 10$–15 km s^{-1}) and shifted towards more negative velocities. This is indicative of contamination of the carbon line with the X line due to emission from elements heavier than carbon. In this table the line-to-continuum ratio (T_l/T_c) is listed as well as the observed Y^+. The electron temperature (derived using eq. [2] of Brown 1980) in column (7) is corrected for the observed Y^+: thus the factor $[(1 + Y^+)^{-0.87}]$ to account for the additional electrons from helium that contribute to the free-free continuum emission is included. The difference between hydrogen and helium velocities (V_{H-He}) is listed in column (9) and the ratio of line width of H to He ($\Delta V_H/\Delta V_{He}$) is listed in column (10). If the helium and hydrogen lines originate from the same volume, V_{H-He} should be zero. Furthermore, since helium is heavier than hydrogen, the helium line should be somewhat narrower than the hydrogen line; $\Delta V_H/\Delta V_{He}$ should be ≥ 1. For comparison, Table 2 gives the same parameters for the global line profiles toward W3A, obtained by integrating the line signal over the entire source.

In Figure 3*b*, the Y^+ distribution based on 110α data (Roelfsema & Goss 1991) is shown with a resolution of 8″. Figure 3*b* shows Y^+ to be between 10% and 15% in the central and eastern parts of W3A, while to the west and south-west Y^+ increases to values locally over 30%. Shaver (1980) has shown that for the determination of electron temperatures in compact H II regions high-frequency radio recombination lines should be used as these are least affected by non–LTE effects. Thus T_e^* as derived from high-frequency lines gives a good representation of the true electron temperature, T_e. Therefore T_e^* was derived from higher frequency H76α data (14.7 GHz) and corrected for the Y^+ distribution derived from the more sensitive 110α observations shown in Figure 3*b*. The resulting distribution of T_e^* is shown in Figure 3*a*. The distribution of T_e^* at 14.7 GHz is quite constant with a mean value of 7500 K and an rms of 750 K. If a constant Y^+ of 10% were assumed, the mean value of T_e^* would be 8500 K with a significantly higher rms of 1500 K. Thus if the assumption is made that the electron temperature is roughly constant throughout W3A, the derived T_e^* distribution shown in Figure 3*a* supports the enhanced values of Y^+ in certain parts of W3A. Clearly the determination of electron temperatures should incorporate the measured values of Y^+.

In addition to confirming the previously measured high values of Y^+, the new more sensitive 92α data also allow the detection of helium lines toward the southern part of W3A. Toward region 4 as indicated in Figure 1, the 92α profile shown in Figure 4 is observed. The profile shows a weak (signal-to-noise ratio of $\sim$6) He92α line. The value of Y^+ as implied by this profile is $Y^+ = 34\% \pm 6\%$. The line parameters of this profile are given in Table 3.

It can be shown that, for optically thin emission, the peak line signal-to-noise ratio for a resolved source is proportional to the ratio of frequency to rms noise in mJy beam^{-1}, ν/σ. For the 76α and 110α data this ratio is less favorable than for the 92α data. In the 76α data, no H line emission is detected toward region 4 at a 3 σ limit of 15 mJy. The 110α data show a weak H line with a peak of 12 ± 3 mJy, but no He line.

3.1. *The Reliability of Y^+ Determinations*

Several observational problems may lead to erroneous results when one is trying to derive accurate abundances of singly ionized helium from radio recombination line observations. (1) The He line and H line emission could be contaminated by emission from radio recombination lines of other elements at similar frequencies; (2) the subtraction of the continuum baseline can seriously affect the line intensities; and (3)

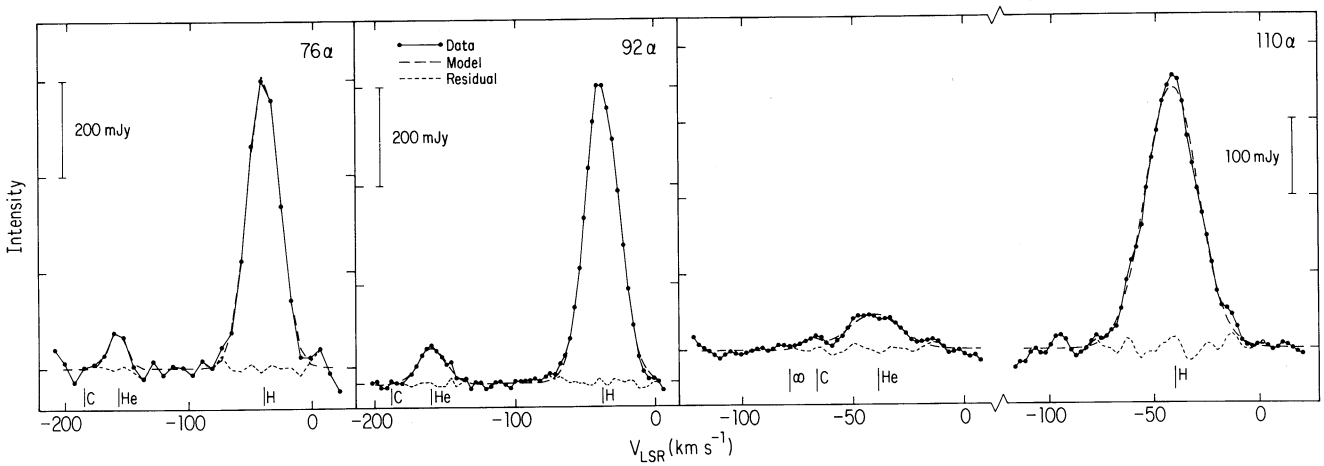

FIG. 2a

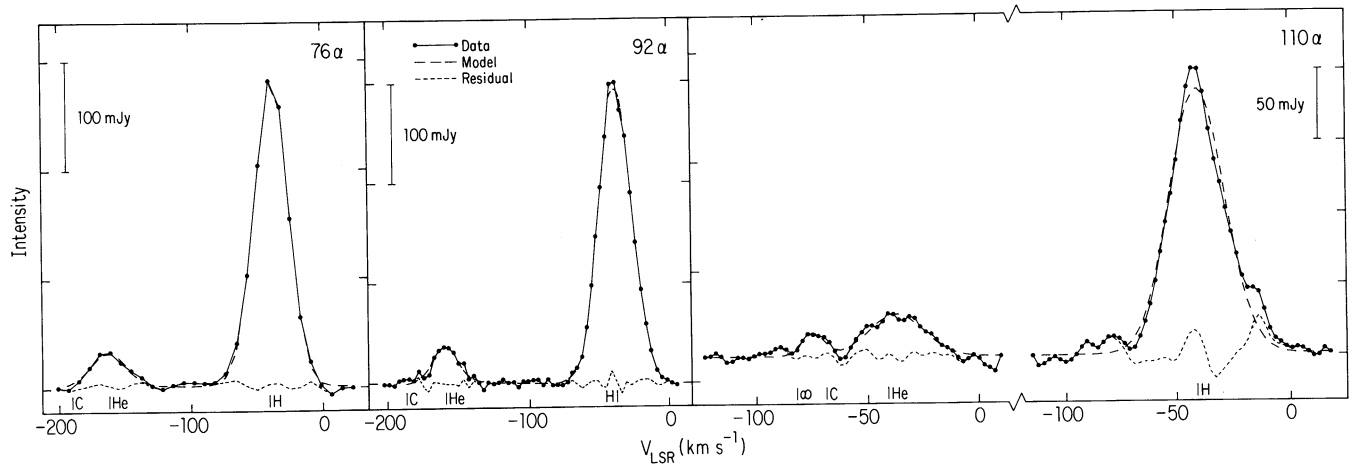

FIG. 2b

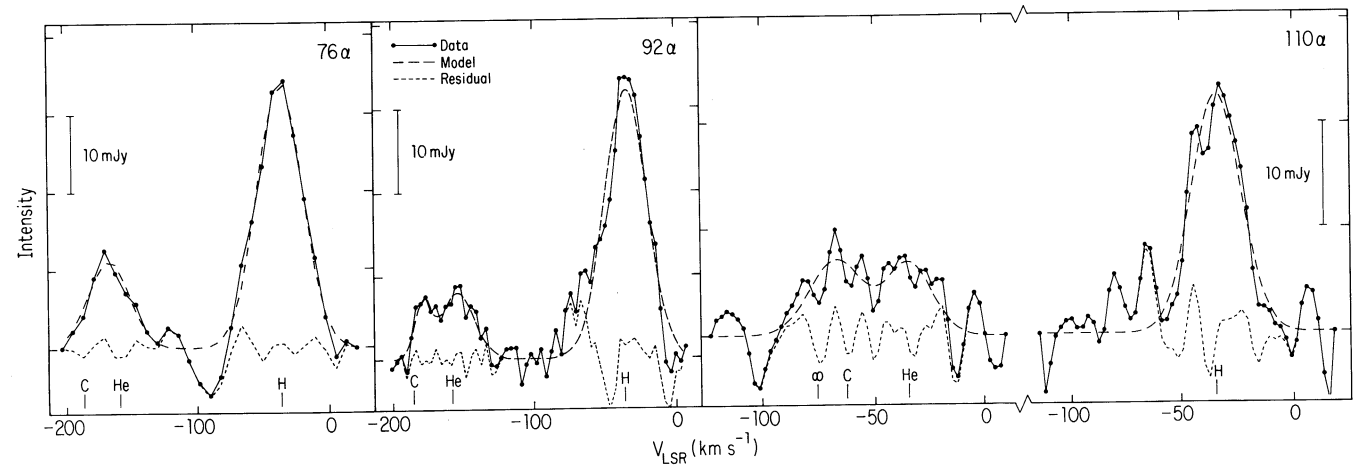

FIG. 2c

FIG. 2.—(*a*) H, He, and C 76α, 92α, and 110α profiles observed toward region 1 (outlined in Fig. 1) in W3A (see text). Fitted Gaussian profiles (H and He for 76α and 92α, H, He, and C for 110α) are indicated by dashed lines. Residuals after subtraction of the best-fit Gaussians are indicated by dotted lines. The abundance of singly ionized helium in this region as implied by these data is $Y^+ = 10\% \pm 2\%$ (Table 1). The velocities of the He and H lines are indicated. Also the expected velocities of the *X* and C lines, using offsets from the He line of 41.1 km s^{-1} and 27.4 km s^{-1} respectively, are indicated. The panels showing the 110α profiles have two velocity scales; one for H and one of He. (*b*) A similar set of profiles obtained toward region 2. These profiles indicate $Y^+ \sim 12\% \pm 2\%$. (*c*) A similar set of profiles obtained toward region 3. These profiles indicate $Y^+ \sim 26\% \pm 5\%$ (here the 92α profile is also fitted with a three-component Gaussian; H, He, and C).

TABLE 1

LINE PARAMETERS FOR RADIO RECOMBINATION LINES OBSERVED TOWARD REGIONS 1, 2, AND 3 IN W3A

Line (1)	Continuum (mJy) (2)	Peak (mJy) (3)	V_{lsr} (km s^{-1}) (4)	ΔV_G (km s^{-1}) (5)	$\frac{T_l}{T_c}$ (6)	$\frac{I(\mathrm{He})}{I(\mathrm{H})}$ (7)	T_e[a] (K) (8)	$V_{\mathrm{H-He}}$ (km s^{-1}) (9)	$\frac{\Delta V_H}{\Delta V_{He}}$ (10)
				Region 1					
H110α	6900	349	−41.9	29.1	5.0%	...	6500	...	...
	(500)	(7)	(0.2)	(0.4)	(0.3)	...	(700)	...	...
He110α	...	47	−40.4	27	0.5	12.3%	...	−1.5	1.1
	...	(6)	(0.8)	(2)	(0.1)	(0.8)	...	(0.9)	(0.1)
H92α	7000	607	−37.5	28.2	8.6	...	6600	...	...
	(200)	(8)	(0.1)	(0.2)	(0.8)	...	(900)	...	...
He92α	...	75	−37.2	22.9	1.1	10.0	...	−0.3	1.2
	...	(8)	(0.6)	(1.6)	(0.1)	(0.7)	...	(0.7)	(0.1)
H76α	4400	623	−38.2	29.6	14.1	...	7800	...	...
	(300)	(18)	(0.4)	(0.9)	(0.9)	...	(900)	...	...
He76α	...	88	−36	16	2.0	7.0	...	−2.2	1.8
	...	(25)	(2)	(5)	(0.5)	(1.8)	...	(2)	(0.5)
				Region 2					
H110α	4100	191	−39.9	27.8	4.6	...	7100	...	...
	(300)	(9)	(0.3)	(0.7)	(0.5)	...	(600)	...	...
He110α	...	30	−36.6	28	0.7	16.0	...	−3.3	1.0
	...	(3)	(0.7)	(2)	(0.1)	(0.9)	...	(0.9)	(0.1)
H92α	3900	299	−36.8	26.9	7.7	...	7700	...	...
	(100)	(4)	(0.1)	(0.2)	(0.1)	...	(500)	...	...
He92α	...	37	−36.2	21.7	0.9	9.9	...	−0.5	1.2
	...	(5)	(0.2)	(1.6)	(0.1)	(0.1)	...	(0.7)	(0.1)
H76α	2200	303	−39.1	27.7	13.7	...	8300	...	...
	(200)	(3)	(0.1)	(0.4)	1.4	...	(800)	...	...
He76α	...	34	−40.1	28	1.5	11.3	...	1.0	1.0
	...	(3)	(1.2)	(3)	(0.2)	(1.2)	...	(1.2)	(0.1)
				Region 3					
H110α	840	24	−33.8	24.8	2.8	...	95000	...	...
	(50)	(3)	(0.3)	(1.7)	(0.4)	...	(1500)	...	...
He110α	...	7	−33	23	0.8	29	...	0.8	1.1
	...	(2)	(3)	(6)	(0.2)	(8)	...	(3)	(0.3)
H92α	578	32	−36.3	34.8	5.6	...	6900	...	...
	(50)	(3)	(0.7)	(1.6)	(0.5)	...	(900)	...	...
He92α	...	8.1	−32.8	27	1.4	20	...	−3.5	1.3
	...	(1.2)	(3.5)	(8)	(0.3)	(5)	...	(3.6)	(0.4)
H76α	460	35	−35.8	38	7.6	...	7200	...	...
	(50)	(2)	(0.9)	(2)	(0.4)	...	(1000)	...	...
He76α	...	12	−44	34	2.6	30	...	−8.3	1.1
	...	(2)	(3)	(6)	(0.4)	(5)	...	(3.1)	(0.2)

NOTE.—Parameters have been corrected for instrumental broadening. Formal 1 σ errors are given in parentheses.
[a] Corrected for Y^+

TABLE 2

GLOBAL LINE PROFILE PARAMETERS FOR RADIO RECOMBINATION LINES OBSERVED TOWARD W3A

Line (1)	Continuum (mJy) (2)	Peak (mJy) (3)	V_{lsr} (km s^{-1}) (4)	ΔV_G (km s^{-1}) (5)	$\frac{T_l}{T_c}$ (6)	$\frac{I(\mathrm{He})}{I(\mathrm{H})}$ (7)	T_e[a] (K) (8)	$V_{\mathrm{H-He}}$ (km s^{-1}) (9)	$\frac{\Delta V_H}{\Delta V_{He}}$ (10)
				Region 1					
H110α	24000	1400	−40.0	28.9	5.8%	...	5700	...	...
	(1000)	(240)	(0.2)	(0.4)	(1.0)	...	(1000)	...	...
He110α	...	184	−39.1	33.4	0.77	14.2%	...	−0.9	0.9
	...	(13)	(0.6)	(1.7)	(0.06)	(0.8)	...	(0.7)	(0.1)
H92α	22500	1850	−36.2	27.0	8.2	...	7800	...	...
	(300)	(25)	(0.1)	(0.2)	(0.4)	...	(600)	...	...
He92α	...	219	−36.7	22.0	1.0	9.6	...	0.5	1.2
	...	(20)	(0.6)	(1.6)	(0.1)	(0.7)	...	(0.7)	(0.1)
H76α	16700	1480	−38.6	28.4	8.9	...	11900	...	...
	(800)	(20)	(0.1)	(0.2)	(0.2)	...	(900)	...	...
He76α	...	177	−39.1	20.9	1.1	8.8	...	0.5	1.4
	...	(15)	(0.6)	(1.4)	(0.1)	(0.9)	...	(0.7)	(0.1)

NOTE.—Parameters corrected for instrumental broadening. Formal 1 σ errors are given in parentheses.
[a] Corrected for Y^+.

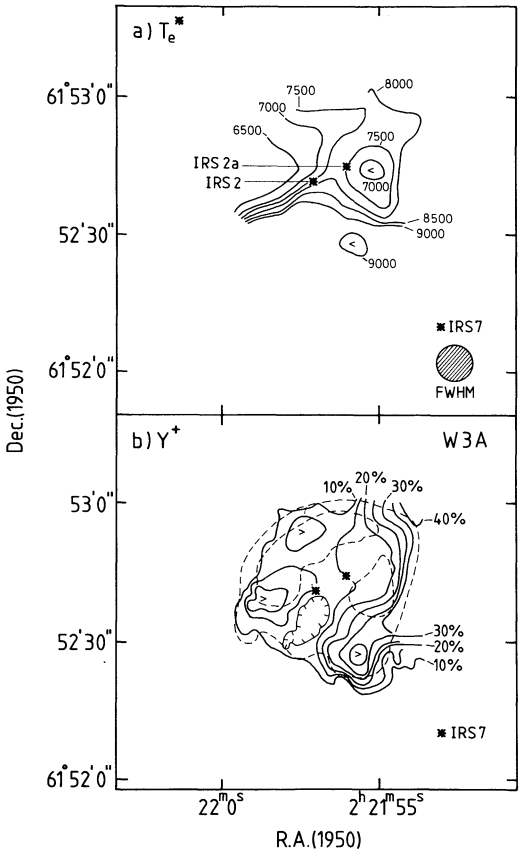

FIG. 3.—(*a*) Distribution of LTE electron temperature T_e^* for W3A derived from the H76α line intensity and the 14.7 GHz continuum, corrected for Y^+ as shown in (*b*). The contour levels are indicated in K. The error in T_e^* is estimated to be 250–500 K in the region north of IRS 2. In the southern third of the source, the error is somewhat higher (up to 1000 K). (*b*) Apparent abundance of singly ionized helium in W3A derived from the H110α and He110α line intensities. The contours are drawn at 10% through 40% with steps of 5% as indicated. Superposed dashed lines are the contours at 150 mJy beam^{-1} and 300 mJy beam^{-1} from the 4.9 GHz continuum map from Roelfsema & Goss (1991). The hatched circle indicates the resolution of 8″. The stars indicate the positions of the infrared sources IRS 2, 2a and 7.

instrumental problems could in principle lead to serious errors in the line shape and thus in Y^+.

1. The most serious possible line contamination is blending of the He line with the neighboring C line. The two lines are separated by 27.4 km s^{-1}; thus in principle, with low spectral resolution, the C line could be confused with the He line. However, the C line typically arises from a cool partially ionized medium and has a width of $\lesssim 5$ km s^{-1}, much less than the typical width of ~ 25 km s^{-1} for the He line (see, e.g., Roelfsema 1987). Thus if the He and C lines were to have the same peak intensity, the intensity of the C line could increase the He line intensity, and thus Y^+, by at most a factor of 1.2. However, given the high spectral resolution of the observations discussed here, such a strong C line would actually be observed in the spectrum and thus would be fitted as a separate line. Indeed, some of the spectra toward positions 1 and 2 (see Fig. 1) show a C line (or a blend of the C and the heavy element line), which does not contribute to the derived He line intensity. Similarly the H line could be contaminated by narrow H° line emission (as observed toward, e.g., K3-50, Roelfsema, Goss, & Geballe 1988). Such contamination would lead to a decrease in the observed Y^+. However, for typical H° lines this decrease would be at most a factor of 1.1.

2. The determination of the baseline for the He and H lines is also clearly critical in obtaining proper line intensities. As an example, if too high a base level is chosen, the integrated line intensity will be underestimated. Therefore, extreme care has been taken in all observations to obtain sufficient channels containing no line emission. As can be seen from the spectra in Figure 2, these baseline levels can be determined at velocities higher than the H line, lower than the He line, and at intermediate velocities between the two lines. In all cases, only a linear continuum level was subtracted. An additional problem may be the erroneous identification of broad line wings (due, e.g., to pressure broadening) at the baseline level. In this case the subtracted continuum level would be too high, and thus the line intensities would be underestimated. However, given the lower peak line intensity of the He line, this would affect the He line intensity more than the H line intensity with a resultant decrease in Y^+.

3. Unspecified instrumental problems could lead to erroneous values of Y^+. In the case of W3A, this is unlikely given the fact that the values of Y^+ are confirmed using two different instruments (VLA and WSRT) and three different transitions (76, 92, and 110α).

TABLE 3

LINES PARAMETERS FOR 92α PROFILE SHOWN IN FIGURE 4

Line	Continuum (mJy)	Peak (mJy)	V_{lsr} (km s^{-1})	ΔV_G (km s^{-1})
H92α.....	380 ± 40	19.8 ± 0.9	−38.5 ± 0.4	23 ± 1
He92α.....	...	5.6 ± 0.9	−37.1 ± 1.8	28 ± 5

4. INTERPRETATION

There appear to be two possible explanations for the observed high values of Y^+. First, these values may reflect

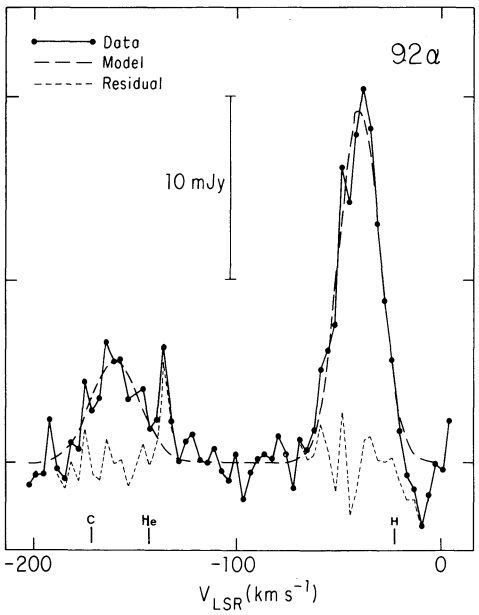

FIG. 4.—The 92α profile as observed toward region 4 as indicated in Fig. 1. The fitted two-component Gaussian profile is indicated by a dashed line. The residual after subtraction of the best-fit Gaussians is indicated by a dotted line. The abundance of singly ionized helium in this region as implied by this profile is $Y^+ = 34\% \pm 6\%$. The line profile parameters are given in Table 3.

actual inhomogeneities in the distribution of helium in W3A. Second, they can be due to variations in the ionization conditions in the H II region. Line transfer effects such as attenuation by continuum optical depth, pressure broadening, stimulated emission, and other non–LTE effects, can most likely be ruled out because these should affect the helium line emission to the same extent as the hydrogen line emission. Thus the ratio of line intensities (Y^+) should not be affected by transfer effects (see, e.g., Brown, Lockman, & Knapp 1978). A possible explanation might also be that the helium and the hydrogen lines originate from different regions with different physical conditions. Then the helium-to-hydrogen ratio may not be related to the local abundance of helium. However, the good agreement between the helium and hydrogen velocities (see Table 1, col. [9] and Roelfsema & Goss 1990) would then be somewhat fortuitous. Regions emitting helium lines would have to mimic very accurately the velocities of the unrelated regions which emit the hydrogen lines.

In the following two sections, enhanced helium abundance and variations in the ionization structure as causes for the high values of Y^+ are discussed in more detail.

4.1. *High Helium Abundance Due to Enrichment of the Local ISM*

High-mass stars are known to undergo mass loss during their evolution. Thus, material processed in the stellar interior is added to the interstellar medium (e.g., Prantzos et al. 1986). As these stars go through a Wolf-Rayet phase, the material ejected into the stellar wind is very rich in helium, and contains virtually no hydrogen. If such an object is (or was) present near W3A, it could have been the source of the helium-rich material. A similar solution has been suggested by Rosa & Mathis (1987) for the observed high helium abundance ($Y^+ \sim 14\%$) in one portion of the 30 Doradus H II region in the Large Magellanic Cloud.

If the mean value of Y^+ for W3A is assumed to be 14% as implied by the 110α data (Table 2, Roelfsema & Goss 1990), the total mass of ionized gas in W3A, as inferred from the continuum flux density, is $M_{\rm tot} = 19\ M_\odot$. Of this total mass, approximately 7 $M_\odot$ is ionized helium. If the primordial helium abundance is 10%, then we expect a maximum helium mass of 4.5 $M_\odot$. The remaining 2.5 $M_\odot$ would have been supplied by a high-mass star. The stellar evolution models of Prantzos et al. (1966) predict that a single star of mass 50 $M_\odot$ would eject 2.2 $M_\odot$ of helium along with a similar amount of hydrogen in its O-star phase. During the Wolf-Rayet phase of its evolution such a star would eject a further 7.9 $M_\odot$ of helium but no additional hydrogen. Clearly such an enrichment (in total 10 $M_\odot$ of helium) of the ISM is more than sufficient to explain the high value of Y^+ as observed in W3A.

Along with the enrichment in helium of the ISM, heavier elements would also be enriched by this mass-loss process. Thus if an evolved object is responsible for the high helium abundance, the metal abundance is also expected to be high near W3A as compared to a nebula showing a lower abundance of He. Prantzos et al. predict enhancements of the O, S, and Ar abundances by a factor of 4 if the ISM were enriched by material ejected from an evolved 50 $M_\odot$ star. In addition the Ne abundance would be increased by an order of magnitude. Thus abundance determinations of these species should allow us to determine whether indeed such enrichement has taken place.

The location of the regions with high Y^+—mainly toward the west and southwest of W3A—suggests that the star or stars which have supplied this enriched material are located to the southwest, just outside of W3A. If either IRS 2 or IRS 2a (located in the center of W3A; see Fig. 1) had been responsible for the overabundance of He, it would seem most likely that Y^+ should be constant, or should decrease with radius. Given the asymmetry in the Y^+ distribution, it seems highly unlikely that either of these stars could be the source of the enriched material.

4.2. *High Helium Abundance Due to Underionization of Hydrogen*

A second way to explain the observations of Y^+ in W3A is by invoking an underabundance of ionized hydrogen rather than an overabundance of helium. We have investigated this problem by considering the ionization structure of hydrogen and helium surrounding hot main-sequence stars. The presence of helium, besides providing additional opacity, produces subtle effects on the ionization structure since the ground-state recombination in helium will not produce diffuse photons which are capable of ionizing hydrogen. Thus the He and H ionization become coupled. The relevant equations are described in Osterbrock (1989). Hummer & Seaton (1963) solved the ionization structure of hydrogen and helium assuming that helium absorbs all the diffuse photons resulting from its ground-state recombinations and the hydrogen ionizations due to bound-bound transitions in helium can be ignored. For stars hotter than $\sim$55,000 K, their solutions showed the presence of a thin shell of ionized helium beyond the hydrogen Strömgren sphere. In later work, notably Rubin's (1986), the transfer problem for diffuse photons was actually solved but the computations were not pursued beyond where hydrogen was still about 90% ionized. Rubin also ignored the effect of helium bound-bound transitions.

Several equilibrium H II region models with existing stars spanning an effective temperature $T_{\rm eff}$ range of 40,000 to 60,000 K were investigated. An ambient density of 10 H atoms cm^{-3} and a helium abundance by number Y of 10% have been used. The stellar fluxes are due to Hummer & Mihalas (1970). For $T_{\rm eff} < 50{,}000$ K, the fluxes beyond the He I ionization limit are low and the He^+ zone always lies within the H^+ zone. At higher temperatures, the boundary of the He^+ zone approaches that of the H^+ zone but never goes beyond it. To understand the deviation from the earlier results, we also computed ionization structures neglecting the effects of helium recombinations of hydrogen ionization as was done by Hummer & Seaton. We do find in these cases a narrow zone of ionized helium where hydrogen is predominantly neutral. Physically, by ignoring the terms that couple hydrogen and helium ionizations, we are artificially suppressing the hydrogen ionization while enhancing the ionization of helium. When these terms are included, the thin ionized helium-neutral hydrogen shell disappears and the ionization zones are practically coincident.

The results of the computations are shown in Figures 5 and 6. Figure 5 shows the ionization structure of hydrogen and helium for an existing star with $T_{\rm eff} = 50{,}000$ K; Figure 6 shows the same for $T_{\rm eff} = 60{,}000$ K. The left-hand panel of each figure illustrates the full solution and the right-hand panel shows the results when the effects of helium recombination on hydrogen ionization are ignored. It seems highly unlikely, therefore, that there will be a significant ionized helium-neutral hydrogen shell at the edges of H II regions exited by main-

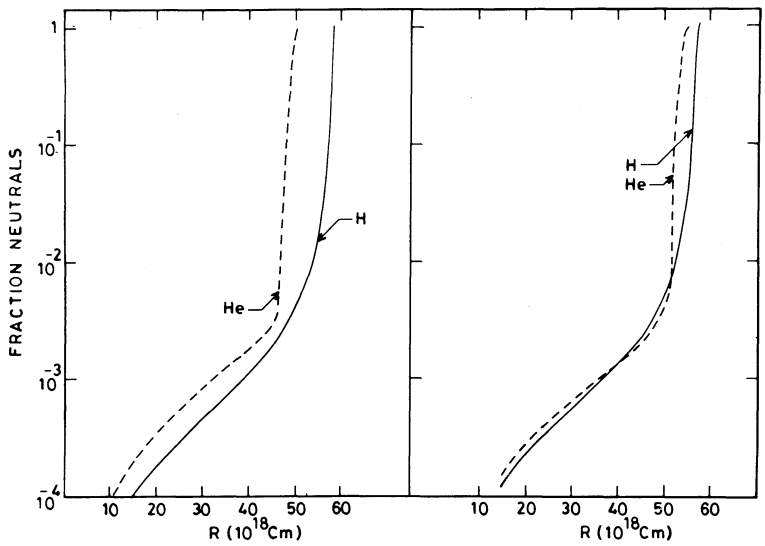

FIG. 5.—Model helium and hydrogen ionization structure of an isothermal H II region ionized by a main-sequence star with $T_{\rm eff}$ 50,000 K. The abundance of helium by number Y is 10%. For the left-hand panel, the effect of helium recombination on hydrogen ionization is included in the calculations; for the right-hand panel, it is not included.

sequence stars. More realistically, all H II regions are expected to contain dust, and in a dusty nebula the coincidence of helium and hydrogen zones is assured because of scattering by dust (see Mathis 1971).

5. CONCLUSIONS

Observations of hydrogen and helium radio recombination line emission toward the Galactic H II region W3A were used to determine the abundance distribution of singly ionized helium Y^+. Locally large enhancements of Y^+ up to $\sim$30% are found. Modelling of H II regions shows that the ionization structure of W3A cannot explain such enhancements. It is concluded that the enhancements in Y^+ most likely reflect an acutal enhancement in the true local helium abundance. An evolved stellar object, located outside of the H II region, could be the source of enriched material.

We are indebted to K. R. Anantharamaiah for a critical reading of an earlier version of the manuscript. We thank R. L. Brown for the stimulating discussions on the interpretation of helium recombination lines and G. Bower for help with the data calibration and reduction. The Westerbork Synthesis Radio Telescope is operated by the Netherlands Foundation for Astronomical Research (ASTRON) which is financially supported by the Netherlands Organization for Scientific Research (N.W.O.). The Very Large Array of the National Radio Astronomy Observatory is operated by Associated Universities Inc. under a cooperative agreement with the National Science Foundation. Roelfsema was supported by the Netherlands Foundation for Astronomical Research (ASTRON).

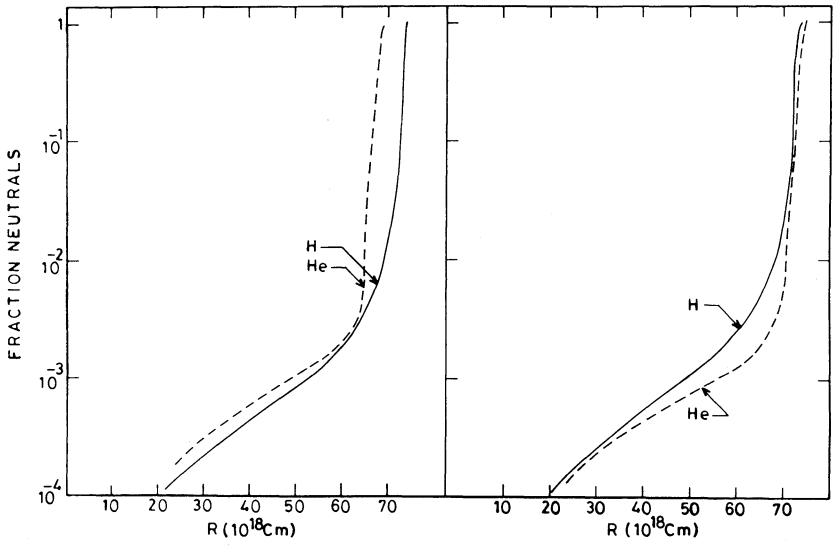

FIG. 6.—Model helium and hydrogen ionization structure of an isothermal H II region ionized by a main-sequence star with $T_{\rm eff}$ 60,000 K. The abundance of helium by number Y is 10%. For the left-hand panel, the effect of helium recombination on hydrogen ionization is included in the calculations; for the right-hand panel, it is not included.

REFERENCES

Bania, T., Rood, R. T., & Wilson, T. L. 1987, ApJ, 323, 30
Brown, R. L. 1980, in Radio Recombination Lines, ed. P. A. Shaver (Dordrecht: Reidel), 53
Brown, R. L., Lockman, F. J., & Knapp, G. R. 1978, ARA&A, 16, 445
Hummer, D. G., & Mihalas, D. M. 1970, MNRAS, 147, 339
Hummer, D. G., & Seaton, M. J. 1963, MNRAS, 127, 217
Mathis, J. S. 1971, ApJ, 167, 261
Mezger, P. G. 1980, in Radio Recombination Lines, ed. P. A. Shaver (Dordrecht: Reidel), 87
Osterbrock, D. E. 1989, Astrophysics of Gaseous Nebulae (Mill Valley, CA: University Science Books)
Prantzos, N., Doom, C., Arnould, M., & de Loore, C. 1986, ApJ, 304, 695
Roelfsema, P. R. 1987, Ph.D. thesis, University of Groningen
Roelfsema, P. R., & Goss, W. M. 1991, A&AS, 87, 177
Roelfsema, P. R., Goss, W. M., & Geballe, T. R. 1988, A&A, 207, 132
———. 1990, A&A, 222, 247
Roelfsema, P. R., Goss, W. M., Whiteoak, J. B., Gardner, F. F., & Pankonin, V. 1987, A&A, 175, 219
Rosa, M., & Mathis, J. S. 1987, ApJ, 317, 163
Rubin, R. H. 1968, ApJ, 153, 761
Shaver, P. A. 1980, A&A, 90, 34
Shaver, P. A., McGee, R. X., Newton, L. M., Danks, A. C., & Pottasch, S. R. 1983, MNRAS, 204, 53
Thum, C., Mezger, P. G., & Pankonin, V. 1980, A&A, 87 269